Chin. J. Mech. Eng. (2017) 30:385–397
DOI 10.1007/s10033-017-0079-3

ORIGINAL ARTICLE

Static and Dynamic Pull-In Instability of Nano-Beams Resting on Elastic Foundation Based on the Nonlocal Elasticity Theory

HAMID M Sedighi[1] · **ASHKAN Sheikhanzadeh**[2]

Received: 29 February 2016 / Revised: 11 October 2016 / Accepted: 11 January 2017 / Published online: 22 March 2017

Abstract This paper provides the static and dynamic pull-in behavior of nano-beams resting on the elastic foundation based on the nonlocal theory which is able to capture the size effects for structures in micron and sub-micron scales. For this purpose, the governing equation of motion and the boundary conditions are driven using a variational approach. This formulation includes the influences of fringing field and intermolecular forces such as Casimir and van der Waals forces. The differential quadrature (DQ) method is employed as a high-order approximation to discretize the governing nonlinear differential equation, yielding more accurate results with a considerably smaller number of grid points. In addition, a powerful analytical method called parameter expansion method (PEM) is utilized to compute the dynamic solution and frequency-amplitude relationship. It is illustrated that the first two terms in series expansions are sufficient to produce an acceptable solution of the mentioned structure. Finally, the effects of basic parameters on static and dynamic pull-in instability and natural frequency are studied.

Keywords Static and dynamic pull-in voltages · Size dependent · Nonlocal theory · Euler–Bernoulli beam model · Differential quadrature method · Parameter Expansion method

✉ HAMID M Sedighi
h.msedighi@scu.ac.ir

[1] Mechanical Engineering Department, Faculty of Engineering, Shahid Chamran University of Ahvaz, Ahvaz 61357-43337, Iran

[2] Departmentof Mechanical Engineering, Najafabad Branch, Islamic Azad Univesity, Najafabad, Iran

1 Introduction

Electrostatically actuated nano-beams play an important role in micro and nano-electromechanical systems (MEMS and NEMS) e.g. biosensors, micro-resonators, atomic force microscopes (AFMs) and actuators [1–4]. MEMS/NEMS may be actuated using several sources of energy such as electrostatic [5], electromagnetic [6], piezoelectric [7] and may be made of metals or polymer, silicon-based structures or functionally graded materials (FGM) [8–13]. Electrostatic actuation has demonstrated good energy density and efficiency. This actuation method transforms electrical energy into motion in order to perform the measurements in the resonators or to act on other components in the microswitches.

Electrostatic resonators are typically as a straight cantilever or a bridge beam having an initial distance from a substrate, actuated by a transverse distributed electrical force caused by the input voltage applied between the beam and substrate. As the applied voltage is increased beyond a critical value, called the pull-in voltage, the instability of beam occurs such that the deflection suddenly raises and the beam contacts with the substrate through the location of maximum deflection. The static and dynamic pull-in behaviors of electrostatically actuated beams have been investigated by several researchers so far. In this regard, Zand and Ahmadian [14] studied the influences of intermolecular forces including Casimir and van der Waals forces on the dynamic pull-in instability of electrostatically actuated beams. Also, the effects of midplane stretching, electrostatic actuation, and fringing fields were considered. The end conditions of the beams were clamped–free and clamped–clamped. Sadeghian et al [15] reported on the pull-in behavior of non-linear microelectromechanical coupled systems. The generalized differential quadrature method was used as a high-order approximation to

discretize the governing nonlinear integro-differential equation. They studied various electrostatically actuated microstructures such as cantilever beam-type and fixed–fixed beam. Hsu [16] presented the nonlinear analysis of nanoelectromechanical systems using the differential quadrature model. The differential quadrature method was applied to overcome the difficulty of determining the nonlinear equation of motion. The characteristics of various combinations of curved electrodes and cantilever beams were considered to optimize the design. Sedighi and Shirazi [17] developed an asymptotic procedure to predict the nonlinear vibrational behavior of micro-beams pre-deformed by an electric field. The nonlinear equation of motion included both even and odd nonlinearities. The parameter expansion method was utilized to obtain the approximated solution and frequency–amplitude relationship. Zare [18] studied the dynamic pull-in instability of functionally graded micro-cantilevers actuated by step DC voltage by considering the fringing-field effect. By employing Homotopy Perturbation Method with an auxiliary term, he obtained the high-order frequency-amplitude relation and investigated the influences of material properties and actuation voltage on dynamic pull-in behavior of microstructures. Sedighi et al [19] studied dynamic pull-in instability of electrostatically-actuated micro-beams by proposing the nonlinear frequency amplitude relationship using Iteration Perturbation Method (IPM). They demonstrated that two terms in series expansions is sufficient to produce an acceptable solution of the micro-structure. Ale Ali et al [20] presented the nonlinear model of a clamped–clamped microbeam actuated by an electrostatic load with stretching and thermoelastic effects. They calculated the frequency of free vibration by discretization based on the differential quadrature (DQ) method and computed the quality factor of thermoelastic damping. In addition, they investigated the variation of thermoelastic damping (TED) versus geometrical parameters, such as thickness, gap distance and the length of micro-beams. Edalatzadeh and Alasty [21] studied the vibration suppression of micro or nano-scale cantilever beams subjected to nonlinear distributed forces such as applied voltage, Casimir, and van der Waals forces. They modeled the nano-beam by strain gradient elasticity theory to account for the size effects of small-scale flexible structures. A novel control law was proposed to guarantee the exponential stability of the linearized closed-loop system and also the local stability of original nonlinear closed-loop system. Then they truncated the continuous model to a set of nonlinear ordinary differential equations by using Kantorovich method. Their simulations showed that the proposed controller not only suppresses the forced vibration of the beam before crossing dynamic pull-in threshold, but also it extends the dynamic pull-in criterion.

Some experimental observations resulted in the size-dependent mechanical behavior in micro-scale structures [22, 23]. Due to the weakness of the classical continuum theory to explain the experimentally-detected small-scale effects in the size dependent behavior of structures, various non-classical theories such as the nonlocal [24], strain gradient [25], and couple stress [26] were introduced to eliminate the shortcoming in dealing with micro and nano-structures. On the basis of the nonlocal continuum mechanics theory [24], the stress at a point is a function of strains at all points in the continuum. This theory includes information about the forces between atoms, and the internal length scale is introduced into the constitutive equations as a material parameter. In recent years, numerous studies including the static, dynamic, and thermal analyses have been accomplished on micro and nano-structures (for instances, see these studies based on the nonlocal [27, 28], strain gradient [29, 30], modified couple stress [31, 32], and non-Fourier heat conduction theories, [33, 34]). Sedighi et al [35] investigated the size dependent electromechanical instability of cantilever nano-actuator by the use of the strain gradient elasticity theory. The nano-actuator was modeled by employing the Euler–Bernoulli beam theory and the equation of motion was derived via Hamilton's principle. The reduced order method (ROM) was applied to solve the nonlinear governing equation. Moreover, static and dynamic pull-in voltages of nano-actuator as functions of dimensionless length scale parameters were determined. They showed that when thickness of the nano-actuator is comparable to the intrinsic material length scales, size effect can substantially influence the pull-in behavior of the system. In other research, Sedighi et al [36] examined the effect of several crucial factors such as finite conductivity, size dependency and surface layer on the electromechanical response and pull-in instability of micro/nano-electromechanical systems. They developed a modified continuum model to incorporate these effects on the dynamic behavior and electromechanical instability of double-sided FGM NEMS bridges. Employing Gurtin–Murdoch model in conjunction with nonlocal Eringen elasticity, the governing equations of the nano-bridges were derived considering the surface layer and size dependency. Also, the Coulomb and Casimir forces were incorporated in the governing equation considering the corrections due to the finite conductivity of FGM (relative permittivity and plasma frequency). Sedighi et al [37] developed a size dependent model for the nonlinear dynamic pull-in instability of a double-sided nano-bridge incorporating the effects of angular velocity and rarefied gas damping. The non-linear governing equation of the nanostructure was derived utilizing Euler-beam model and Hamilton's principle including the dispersion forces. In addition, the strain gradient elasticity theory was applied

for modeling the size-dependent behavior of the system. The reduced order method was also implemented to discretize and solve the partial differential equation of motion. Sedighi et al [38] investigated the dynamic pull-in instability of vibrating micro-beams undergoing large deflection under electrostatically actuation. The governing nonlinear equation of motion was obtained based on the modified couple stress theory. Homotopy Perturbation Method was used to present the high accuracy approximate solution as well as the second-order frequency- amplitude relationship. Tadi Beni [39] developed the nonlinear formulation of functionally graded piezoelectric nanobeam by applying the Euler–Bernoulli model and using the consistent size-dependent theory. The power-law distribution rule was assumed for the mechanical properties in beam thickness and the effects of electrical force, mechanical force and material properties of functionally graded piezoelectric beam on the static responses, buckling, and free vibrations were discussed. By incorporating the Timoshenko beam theory and nonlocal Eringen-like constitutive law, a new formulation for size-dependent Timoshenko nanobeams described by Barretta et al [40] on the basis of two material length-scale model. They also established new closed form solutions of nonlocal Timoshenko nanobeams. Karimi et al [41] studied the size-dependent free vibration characteristics of rectangular nanoplates considering the surface stress effects by employing finite difference method (FDM). They employed the Gurtin–Murdoch continuum elasticity approach to include the surface effects in the nonlinear equations of motion. They also demonstrated the difference between the natural frequency obtained by considering the surface effects and that obtained without considering surface properties and observed that the effects of surface properties tend to diminish in thicker nanoplates, and vice versa. The size-dependent dynamic instability of suspended nanowires in the presence of Casimir force and surface effects was presented by Sedighi and Bozorgmehri [42]. The Casimir-induced instability of nanowires with circular cross-section was modeled by cylinder-plate geometry assumption. To express the Casimir attraction of cylinder-plate geometry, they employed the proximity force approximation (PFA) for small separations and Dirichlet asymptotic approximation for large separations and utilized a step-by-step numerical method for solving a nonlinear problem. It was observed that the phase portrait of Casimir-induced nanowires exhibit periodic and homoclinic orbits. Karimpour et al [43] investigated the size-dependent instability of double-sided nano-actuators using couple stress theory (CST) in the presence of Casimir force. To solve the governing equations, they applied the differential transformation method (DTM) and calculated the critical deflection and pull-in voltage of the nanostructures.

This paper tries to fulfill the gap in the open literature by finding the static and dynamic pull-in voltages of nano-beam resonator utilizing the nonlocal continuum mechanics theory. To this aim, the size-dependent motion equation and boundary conditions of nano-beams resting on the elastic foundation are derived using a variational approach. The differential quadrature (DQM) and Parameter Expansion (PEM) methods are employed to solve the governing nonlinear differential equation and estmate the static and dynamic pull-in behaviors. Finally, the effects of basic parameters such as the internal characteristic length, intermolecular forces and the stiffness of foundation on the static and dynamic pull-in instability are investigated.

2 Basic Formulation

2.1 Preliminaries

The most of electrostatically actuated nano-resonators are modeled as elastic beams with rectangular cross-sections, as shown in Fig. 1. The nano-beam has length L, thickness h, width b, density ρ, and a modulus of elasticity E. The parameter d is the initial gap between the nano-beam and substrate. Furthermore, the coordinate system is composed of the beam axis (the x coordinate), and axes correspond to the width and thickness (the y and z coordinates), respectively. Moreover, the origin is placed at the centroid of the cross section in the right hand side of the beam.

On the basis of Euler–Bernoulli beam model, the cross-sections of the beam remain planar and perpendicular to the bending axis after deformation. Hence, the components of the displacement vector field, $\boldsymbol{u} = (u_x,\ u_y,\ u_z)$ can be defined as follows:

$$u_x = -z\,\frac{\partial w(x,t)}{\partial x},\quad u_2 = 0,\quad u_3 = w(x,t), \tag{1}$$

Where, the function $w(x,t)$ indicates transverse deflection of the beam cross-sections. In addition, parameter t denotes the time.

According to the nonlocal theory [24], the stress field at a point in an elastic continuum not only depends on the

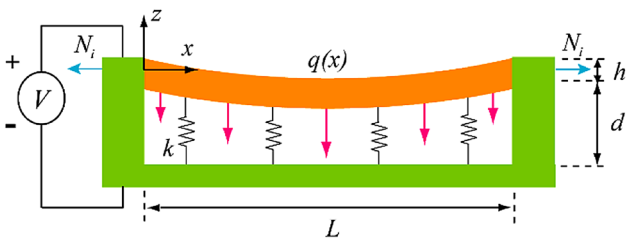

Fig. 1 Electrostatically actuated nano-beam resonator configuration, coordinate system and geometric characteristics

strain field at the point but also on strains at all other points of the body.

According to this theory, the nonlocal constitutive equation of a Hookean solid can be expressed as follows [24]

$$(1-(e_0a)^2\nabla^2)\sigma_{ij}=C_{ijmn}\varepsilon_{mn} \tag{2}$$

Where

$$\varepsilon_{mn}=\frac{1}{2}\left(\frac{\partial u_m}{\partial x_n}+\frac{\partial u_n}{\partial x_m}\right), \tag{3}$$

and C_{ijmn}'s are the components of the fourth-order elasticity tensor, as well as parameters e_0 and a denote the material constant and the internal characteristic length, respectively. Also, the variation of the strain energy δU for an anisotropic linear elastic material occupying region Ω can be written as [25]:

$$\delta U=\int_{\Omega}\sigma_{ij}\delta\varepsilon_{ij}\,d\Omega. \tag{4}$$

In which, σ_{ij} and ε_{ij} represent the components of the nonlocal stress and strain tensors.

2.2 The dynamic equilibrium equation

Substituting components of displacement vector from Eq. (1) into Eq. (3) results in the following nonzero strain components as

$$\varepsilon_{xx}=-z\frac{\partial^2 w(x,t)}{\partial x^2}. \tag{5}$$

By inserting Eq. (5) into Eq. (4) and taking integral by parts on the ensuing relation, the variation of strain energy of nano-beam can be readily obtained as [44]

$$\delta U=\int_0^L-\left(\frac{\partial^2 M_{xx}}{\partial x^2}\right)\delta w(x,t)dx+\left(\frac{\partial M_{xx}}{\partial x}\delta(w(x,t))\right)_{x=0}^{x=L}-\left(M_{xx}\delta(\frac{\partial w(x,t)}{\partial x})\right)_{x=0}^{x=L}. \tag{6}$$

In Eq. (6), we have [44]

$$\frac{\partial^2 M_{xx}}{\partial x^2}-(e_0a)^2\frac{\partial^4 M_{xx}}{\partial x^4}=-EI\frac{\partial^4 w(x,t)}{\partial x^4}. \tag{7}$$

Where $I=bh^3/12$ is the inertia moment of the cross-section. On the other hand, the variation of the kinetic energy within the Euler–Bernoulli beam model can be computed from the following relation [45]:

$$\delta(K.E)=\rho\int_0^L\left[\left(I\frac{\partial^2\ddot{w}}{\partial x^2}-A\,\ddot{w}\right)\delta w(x,t)\right]+\frac{\partial}{\partial t}\left(I\frac{\partial\dot{w}}{\partial x}\delta\left(\frac{\partial w}{\partial x}\right)+A\dot{w}\,\delta w\right)\Bigg]dx \tag{8}$$

in which A is cross-sectional area of the beam. The virtual work done by the axial load, electrostatic voltage, elastic foundation and the intermolecular force can be expressed as:

$$W=\frac{1}{2}\int_0^L\left(N_i+\frac{EA}{2L}\int_0^L w_x^2dx\right)w_x^2dx+\int_0^L\left[F_e+(F_C\,or\,F_V\,)-k\,w\right]w\,dx, \tag{9}$$

where N_i is the axial force and

$$F_e=\frac{1}{2}b\,\varepsilon_0\left(\frac{V}{d-w}\right)^2\left(1+\hat{f}\frac{d-w}{b}\right),\qquad F_C=\frac{\pi^2\hbar\,c\,b}{240(d-w)^4},\quad F_V=\frac{\Lambda b}{6\pi(d-w)^3}. \tag{10}$$

In Eq. (10), the term $\hat{f}=0.65$ is the fringing field effect due to the finite width of the beam and parameter $\varepsilon_0=8.854\times10^{-12}(\mathrm{C^2N^{-1}m^{-2}})$ is the vacuum permittivity. Also, $\hbar=1.055\times10^{-34}(\mathrm{Js})$ and $c=2.998\times10^{8}(\mathrm{m/s})$ indicate the Planck's constant divided by 2π and the speed of light, respectively. Moreover, $\Lambda=0.4\times10^{-19}$ is the Hamaker constant.

The outcomes obtained for the variation of the strain energy from Eq. (6), the variation of the kinetic energy from Eq. (8) and the variation of the virtual work from Eq. (9) are substituted into the equation of the Hamilton principle on the time interval between t_1 and t_2:

$$\int_{t_1}^{t_2}(\delta(K.E)-\delta U+\delta W)dt=0. \tag{11}$$

Since δw is arbitrary at all points of the nano-beam, the governing motion equation of a electrostatically actuated nano-bridge resting on the elastic foundation and including influences of intermolecular forces can be obtained as follows:

$$\frac{\partial^2 M_{xx}}{\partial x^2}+\rho\left(I\frac{\partial^2\ddot{w}(x,t)}{\partial x^2}-A\ddot{w}(x,t)\right)+\left(N_i+\frac{Ebh}{2L}\int_0^L\left(\frac{\partial w(x,t)}{\partial x}\right)^2dx\right)\frac{\partial^2 w(x,t)}{\partial x^2}+F_e+(F_C\,or\,F_V\,)-k\,w=0. \tag{12}$$

Also, the boundary conditions at points on the end edges at $x=0$ and L can be expressed as:

$$\frac{\partial M_{xx}}{\partial x}=0,\quad or\quad \delta w=0\qquad M_{xx}=0,\quad or\quad \delta\left(\frac{\partial w}{\partial x}\right)=0. \tag{13}$$

Finally, using Eqs. (7) and (12), the governing equation of motion in terms of transverse deflection w can be written as

$$EI\frac{\partial^4 w}{\partial x^4} = \left(1-(e_0a)^2\frac{\partial^2}{\partial x^2}\right) \times \left[\left(N_i + \frac{Ebh}{2L}\int_0^L \left(\frac{\partial w(x,t)}{\partial x}\right)^2 dx\right)\frac{\partial^2 w(x,t)}{\partial x^2} + F_e + \rho I\frac{\partial^2 \ddot{w}}{\partial x^2} - \rho A\ddot{w} - k\,w + (F_V \text{ or } F_C)\right]. \tag{14}$$

In order to normalize the governing equation, the following dimensionless quantities are defined as:

$$\tilde{w} = \frac{w}{d}, \quad \zeta = \frac{x}{L}, \quad \tau = \sqrt{\frac{EI}{\rho AL^4}}t. \tag{15}$$

By employing these dimensionless parameters, the normalized form of the motion equation is:

$$\frac{\partial^4 \tilde{w}}{\partial \zeta^4} = \left(1-(e_0a)^{*2}\frac{\partial^2}{\partial \zeta^2}\right) \times \left(\eta\frac{\partial^2 \tilde{w}}{\partial \tau^2 \partial \zeta^2} - \frac{\partial^2 \tilde{w}}{\partial \tau^2} - k^*\tilde{w} + \left(f_i + \alpha\int_0^1 \left(\frac{\partial \tilde{w}}{\partial \xi}\right)^2 d\xi\right) \times \frac{\partial^2 \tilde{w}}{\partial \xi^2} + \frac{(V_0^*)^2}{(1-\tilde{w})^2}\left(1+\hat{f}^*(1-\tilde{w})\right) + \left(\frac{\Lambda^*}{(1-\tilde{w})^3} \text{ or } \frac{(\hbar c)^*}{(1-\tilde{w})^4}\right)\right), \tag{16}$$

In which

$$(e_0a)^* = \frac{e_0a}{L}, \quad \eta = \frac{I}{AL^2}, \quad k^* = \frac{kL^4}{EI}, \quad V_0^* = V_0\sqrt{\frac{b\varepsilon_0 L^4}{2EId^3}}, \quad \hat{f}^* = \hat{f}\frac{d}{b}, \quad \Lambda^* = \frac{\Lambda L^4}{6\pi EId^4}. \quad (\hbar c)^* = \frac{\pi^2 \hbar c b L^4}{240EId^5}, \quad \alpha = 6\left(\frac{d}{h}\right)^2, \quad f_i = \frac{N_i L^2}{EI} \tag{17}$$

3 Solution Methodology

In this section, two numerical and analytical methods are used to solve the governing nonlinear differential equation presented in Eq. (16). First, the differential quadrature method as an efficient and accurate numerical method is employed to discretize the nonlinear differential equation and to reduce the static equation to a set of algebraic equations. Next, to solve the dynamic equation of motion, the parameter expansion method as a powerful analytical method in conjunction with Bubnov-Galerkin procedure are utilized to obtain the normalized natural frequency and the dynamic solution.

3.1 Differential Quadrature Method (DQM)

Based on the differential quadrature method, the derivative of a function at each point of the domain can be approximated as a weighted linear summation of the values of the function at all of the sample points in the domain. Employing this approximation, the differential equations are reduced to a set of algebraic equations. The number of equations depends on the selected number of sample points.In this study, the differential quadrature approximation to the mth-order derivative of function $\tilde{w}(\zeta)$ at the ith sampling point is given by [15]:

$$\begin{bmatrix} \left.\frac{\partial^m \tilde{w}(\zeta)}{\partial \zeta^m}\right|_{\zeta=\zeta_1} \\ \cdot \\ \cdot \\ \cdot \\ \left.\frac{\partial^m \tilde{w}(\zeta)}{\partial \zeta^m}\right|_{\zeta=\zeta_N} \end{bmatrix} \cong \left[D_{ij}^m\right] \begin{bmatrix} \tilde{w}(\zeta_1) \\ \cdot \\ \cdot \\ \cdot \\ \tilde{w}(\zeta_N) \end{bmatrix} \quad for\ i,j = 1,2,\ldots,N \tag{18}$$

where $\tilde{w}(\zeta_i)$ is the value of the function at the sample point ζ_i and $D_{ij}^{(m)}$ are the weighting coefficients of the mth-order differentiation that is attached to these functional values. The function $\tilde{w}(\zeta)$ is defines as [15]:

$$\tilde{w}(\zeta) = \sum_{i=1}^{N} \frac{\varphi(z)}{(z-z_i)\varphi_1(z_i)}\tilde{w}(\zeta_i) \tag{19}$$

where

$$\varphi(z) = \prod_{j=1}^{N}(z-z_j), \quad \varphi_1(z_i) = \prod_{j=1,j\neq i}^{N}(z_i-z_j) \quad for\ \ i = 1,2,\ldots,N \tag{20}$$

$$z_i = \frac{L}{2}\left(1-\cos\frac{(i-1)\pi}{N-1}\right) \quad for\ \ i = 1,2,\ldots,N.$$

Substituting Eq. (19) into Eq. (18) yields:

$$D_{ij}^{(1)} = \frac{\varphi_1(z_i)}{(z_i-z_j)\varphi_1(z_j)} \quad for\ \ i,j = 1,2,\ldots,N \text{ and } i \neq j$$

$$D_{ii}^{(1)} = -\sum_{j=1,j\neq i}^{N} D_{ij}^{(1)} \quad for\ \ i,j = 1,2,\ldots,N. \tag{21}$$

Furthermore, higher-order derivatives of differential quadrature weighting coefficients can be expressed by matrix multiplication:

$$D_{ij}^{(2)} = \sum_{k=1}^{N} D_{ik}^{(1)} D_{kj}^{(1)} \quad for\ \ i,j = 1,2,\ldots,N$$
$$D_{ij}^{(3)} = \sum_{k=1}^{N} D_{ik}^{(1)} D_{kj}^{(2)} \quad for\ \ i,j = 1,2,\ldots,N \tag{22}$$
$$D_{ij}^{(4)} = \sum_{k=1}^{N} D_{ik}^{(1)} D_{kj}^{(3)} \quad for\ \ i,j = 1,2,\ldots,N.$$

$$\frac{(V_0^*)^2}{(1-\tilde{w})^2}\left(1+\hat{f}^*(1-\tilde{w})\right) \cong (V_0^*)^2\left[\left(1+2\tilde{w}+3\tilde{w}^2+4\tilde{w}^3+\cdots\right)\right.$$
$$\left.+\hat{f}^*\left(1+\tilde{w}+\tilde{w}^2+\tilde{w}^3+\cdots\right)\right]$$
$$\frac{\Lambda^*}{(1-\tilde{w})^3} \cong \Lambda^*\left(1+3\tilde{w}+6\tilde{w}^2+10\tilde{w}^3+\cdots\right)$$
$$\frac{(\hbar c)^*}{(1-\tilde{w})^4} \cong (\hbar c)^*\left(1+4\tilde{w}+10\tilde{w}^2+20\tilde{w}^3+\cdots\right). \tag{25}$$

Substituting the normalized terms of F_e, F_C, and F_V from Eq. (25) into Eq. (16) yields:

$$\frac{\partial^4\tilde{w}}{\partial\zeta^4} - \left(1-(e_0a)^{*2}\frac{\partial^2}{\partial\zeta^2}\right)\left[\eta\frac{\partial^2\tilde{w}}{\partial\tau^2\partial\zeta^2} - \frac{\partial^2\tilde{w}}{\partial\tau^2} - k^*\tilde{w} + \left(f_i + \alpha\int_0^1\left(\frac{\partial\tilde{w}}{\partial\xi}\right)^2 d\xi\right)\frac{\partial^2\tilde{w}}{\partial\xi^2}\right.$$
$$+\ (V_0^*)^2\left(1+\hat{f}^*\right)\ +\Lambda^*+(\hbar c)^* + \left((V_0^*)^2(2+\hat{f}^*)+3\Lambda^*+4(\hbar c)^*\right)\tilde{w}$$
$$\left.+\left((V_0^*)^2(3+\hat{f}^*)+6\Lambda^*+10(\hbar c)^*\right)\tilde{w}^2+\left((V_0^*)^2(4+\hat{f}^*)+10\Lambda^*+20(\hbar c)^*\right)\tilde{w}^3+\cdots\right] = 0. \tag{26}$$

3.2 Parameter Expansion Method

In this section, the parameter expansion method with the aid of Bubnov–Galerkin decomposition method is employed to solve the dynamic governing equation. To this purpose, the dimensionless transverse deflection of beam is defined as follows:

$$\tilde{w}(\zeta,\tau) = \phi(\zeta)q(\tau), \tag{23}$$

where $\phi(\zeta)$ is the first shape mode of the clamped–clamped beam which can be readily obtained as:

$$\phi(\zeta) = (\cosh\lambda\zeta - \cos\lambda\zeta) - \frac{\cosh\lambda-\cos\lambda}{\sinh\lambda-\sin\lambda}(\sinh\lambda\zeta-\sin\lambda\zeta). \tag{24}$$

In which, λ is the first root of characteristic equation. The normalized terms of F_e, F_C, and F_V in Eq. (16) can be approximated by Taylor's series as:

By applying the Bubnov–Galerkin method, one can obtain:

$$\int_0^1\left\{\frac{\partial^4\tilde{w}}{\partial\zeta^4} - \left(1-(e_0a)^{*2}\eta^2\frac{\partial^2}{\partial\zeta^2}\right)\left[\frac{\partial^2\tilde{w}}{\partial\tau^2\partial\zeta^2} - (12/\eta^2)\frac{\partial^2\tilde{w}}{\partial\tau^2} - k^*\tilde{w} + \left(f_i+\alpha\int_0^1\left(\frac{\partial\tilde{w}}{\partial\xi}\right)^2 d\xi\right)\frac{\partial^2\tilde{w}}{\partial\xi^2}\right.\right.$$
$$+\ (V_0^*)^2\left(1+\hat{f}^*\right)\ +\Lambda^*+(\hbar c)^* + \left((V_0^*)^2(2+\hat{f}^*)+3\Lambda^*+4(\hbar c)^*\right)\tilde{w} + \left((V_0^*)^2(3+\hat{f}^*)\right.$$
$$\left.\left.+6\Lambda^*+10(\hbar c)^*\right)\tilde{w}^2+\left((V_0^*)^2(4+\hat{f}^*)+10\Lambda^*+20(\hbar c)^*\right)\tilde{w}^3+\cdots\right]\Big\}\phi(\zeta)d\zeta = 0. \tag{27}$$

By inserting Eqs. (23) into (27), the non-dimensional nonlinear equation of motion can be obtained as:

$$\frac{d^2q}{d\tau^2} + \beta_1 q + \left[\beta_2 q^2 + \beta_3 q^3 + \beta_4 q^4 + \beta_0\right] = 0. \tag{28}$$

Here the parameters $\beta_i (i = 0,\ldots,4)$ can be found in the Appendix A. Consider Eq. (28) for the free vibration of a nano-beam with the following general initial conditions:

$$q(\tau=0) = A, \quad \frac{dq}{d\tau}(\tau=0) = 0. \tag{29}$$

It is noticed that free vibration of the system is a periodic motion and can be stated by the base functions $\cos(m\omega\tau)$ $(for\ m = 1,2,\ldots)$. Where, the dimensionless angular frequency of oscillation is indicated by ω.

Table 1 Comparison between the static and dynamic pull-in voltages of nano-beams predicted by classical theory with the numerical and experimental results given by Rezazadeh et al [46] and Osterberg [47], respectively

Static pull-in voltage			Dynamic pull-in voltage		
Present study (DQM)	Rezazadeh et al [46].	Osterberg [47]	Present study (ROM)	Rezazadeh et al [46].	Osterberg [47]
4.73	4.8	4.8	4.36	4.35	4.40

Table 2 A comparison between dynamic pull-in voltages calculated by different methods

Method	Present analysis (Numerical results)	Reduced order model [48]	Finite difference [48]	Three modes assumption [50]
V_{pid}	41.71	41.68	41.61	41.85

Table 3 Comparison between fundamental frequencies of micro-beams calculated by different methods

Beam length (μm)	D.C. voltage (V)	$\omega/2\pi$ (kHz)				
		Present analysis (PEM)	Measured [49]	Calculated [49]	Calculated [51]	HAM [52]
210	6.0	324.71	322.05	324.70	324.70	324.78
310	3.0	163.96	163.22	164.35	163.46	163.16
410	3.0	103.74	102.17	103.80	103.70	103.42

Furthermore, one of our major goal is to determine $\omega(A)$ as a function of the initial amplitude A. In the parameter expansion method, an artificial perturbation equation is formed by embedding an artificial parameter $p\varepsilon[0,1]$ which is employed as an expanding parameter. Based on the PEM, the function q is expanded into a series of p in the form

$$q(\tau,p)=\sum_{i=0}^{\infty}p^{i}q_i(\tau). \tag{30}$$

Moreover, the coefficients **1** and β_1 in Eq. (28) should be expanded in a similar way:

$$\begin{aligned}1&=1+pa_1+p^2a_2+\cdots,\\ \beta_1&=\omega^2-pb_1-p^2b_2-\cdots,\\ 1&=pc_1+p^2c_2+\cdots.\end{aligned} \tag{31}$$

In Eq. (31), a_i, b_i and c_i $(i=1,2,\ldots)$ are to be determined. For $p=0$, Eq. (28) becomes a linear differential equation as well as the approximate solution of nonlinear Eq. (28) can be obtained by $p=1$. Substituting Eqs. (30) and (31) into Eq. (28) results in:

$$\begin{aligned}&(1+pa_1)\frac{d^2}{d\tau^2}(q_0+pq_1)+(\omega^2-pb_1)(q_0+pq_1)\\ &\quad=(pc_1+p^2c_2)\left[\beta_2(q_0+pq_1)^2+\beta_3(q_0+pq_1)^3\right.\\ &\quad\left.+\beta_4(q_0+pq_1)^4+\beta_0\right]\end{aligned} \tag{32}$$

Collecting the terms of the same power of p in Eq. (32), a set of linear equations can be obtained as follow

Table 4 A comparison between dynamic pull-in voltages of typical microbeam

Method	Present modelling (numerical results)	Experiment [53]	Finite difference [54]
V_{pid}	98.1	100	99–100

$$\begin{aligned}&p^0:\frac{d^2q_0}{d\tau^2}+\omega^2q_0=0,\ q_0(\tau=0)=A,\ \frac{dq_0}{d\tau}(\tau=0)=0.\\ &p^1:\frac{d^2q_1}{d\tau^2}+\omega^2q_1=-a_1\frac{d^2q_0}{d\tau^2}+b_1q_0\\ &+c_1\beta_2\left[\beta_2q_0^2(q_0)^2+\beta_3q_0^3+\beta_4q_0^4+\beta_0\right]\\ &with\quad q_1(\tau=0)=0,\ \frac{dq_1}{d\tau}(\tau=0)=0.\end{aligned} \tag{33}$$

Solving the first equation in Eq. (33) yields

$$q_0=A\cos(\omega\tau). \tag{34}$$

Inserting q_0 from Eq. (34) into the right-hand side of second term in Eq. (33) gives:

$$\begin{aligned}&\frac{d^2q_1(\tau)}{d\tau^2}+\omega^2q_1(\tau)=\left(b_1+a_1\omega^2-\frac{3}{4}c_1\beta_3A^2\right)A\cos(\omega\tau)\\ &-\frac{c_1}{2}\left(\beta_4A^2+\beta_2\right)A^2\cos(2\omega\tau)-\frac{1}{4}c_1\beta_3A^3\cos(3\omega\tau)\\ &-\frac{1}{8}c_1\beta_4A^4\cos(4\omega\tau)-\frac{1}{2}c_1\beta_2A^2-\frac{3}{8}c_1\beta_4A^4-c_1\beta_0.\end{aligned} \tag{35}$$

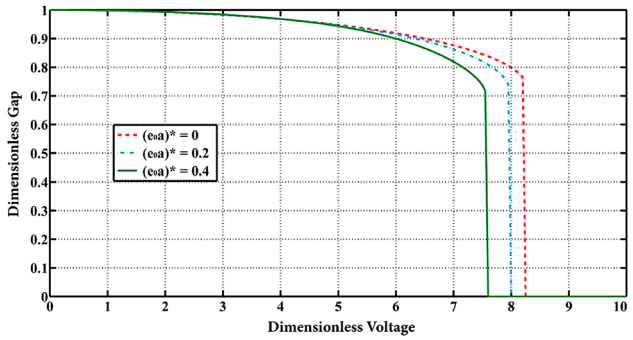

Fig. 2 Maximum dimensionless deflection of the nano-beam versus input voltage for various values of the normalized internal parameter $(e_0a)^*$

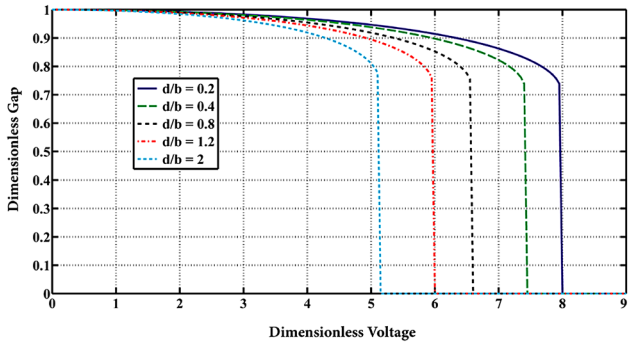

Fig. 3 Maximum dimensionless deflection of the nano-beam versus input voltage for various values of aspect ratio *d/b*

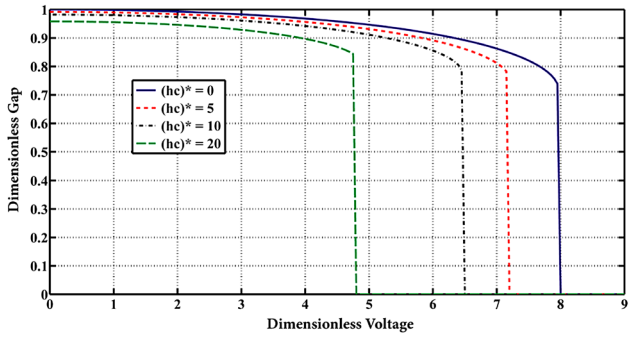

Fig. 4 Maximum dimensionless deflection of the nano-beam versus input voltage for various values $(hc)^*$

By eliminating the secular term (the coefficient of $\cos(\omega\tau)$) in the right-hand side of Eq. (35), one can get

$$b_1 + a_1\omega^2 - \frac{3}{4}c_1\beta_3 A^2 = 0. \tag{36}$$

For two terms approximation of series respect to p in Eq. (31) and considering $p = 1$, we obtain

$$a_1 = 0, \qquad \beta_1 = \omega^2 - b_1, \qquad c_1 = 1. \tag{37}$$

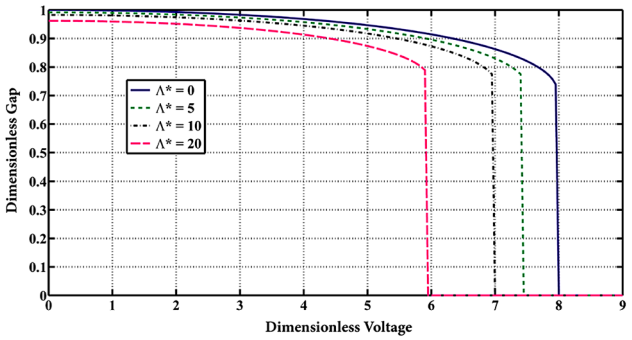

Fig. 5 Maximum dimensionless deflection of the nano-beam versus input voltage for various values Λ*

By use of Eqs. (36) and (37), the dimensionless angular frequency of oscillation can be readily found as follows

$$\omega(A) = \pm\sqrt{\beta_1 + \frac{3}{4}\beta_3 A^2}. \tag{38}$$

By solving Eq. (35), the function $q_1(\tau)$ can be obtained as

$$q_1(\tau) = q_1^h(\tau) + q_1^p(\tau), \tag{39}$$

in which

$$\begin{aligned} q_1^h(\tau) &= C\cos(\omega\tau) + D\sin(\omega\tau), \\ q_1^p(\tau) &= \frac{c_1(\beta_4 A^2 + \beta_2)A^2}{6\omega^2}\cos(2\omega\tau) \\ &+ \frac{c_1\beta_3 A^3}{32\omega^2}\cos(3\omega\tau) + \frac{c_1\beta_4 A^4}{120\omega^2}\cos(4\omega\tau) \\ &- \frac{c_1(3\beta_4 A^2 + 4\beta_2)A^2 + 8c_1\beta_0}{8\omega^2}. \end{aligned} \tag{40}$$

In Eq. (40), C and D are the unknown coefficients which can be computed by imposing the initial conditions in Eq. (33) as follows:

$$\begin{aligned} C &= \frac{c_1(96\beta_4 A^2 + 160\beta_2)A^2 - 15c_1\beta_3 A^3 + 480c_1\beta_0}{480\omega^2}, \\ D &= 0. \end{aligned} \tag{41}$$

Therefore, the following second order approximation for function $q(\tau)$ is as

$$\begin{aligned} q(\tau) = A\cos(\omega\tau) &+ \frac{c_1(96\beta_4 A^2 + 160\beta_2)A^2 - 15c_1\beta_3 A^3 + 480c_1\beta_0}{480\omega^2}\cos(\omega\tau) \\ &+ \frac{c_1(\beta_4 A^2 + \beta_2)A^2}{6\omega^2}\cos(2\omega\tau) \\ &+ \frac{c_1\beta_3 A^3}{32\omega^2}\cos(3\omega\tau) + \frac{c_1\beta_4 A^4}{120\omega^2}\cos(4\omega\tau) \\ &- \frac{c_1(3\beta_4 A^2 + 4\beta_2)A^2 + 8c_1\beta_0}{8\omega^2}, \\ &\times \textit{with}\ \ \omega(A) = \sqrt{\beta_1 + \frac{3}{4}\beta_3 A^2}. \end{aligned} \tag{42}$$

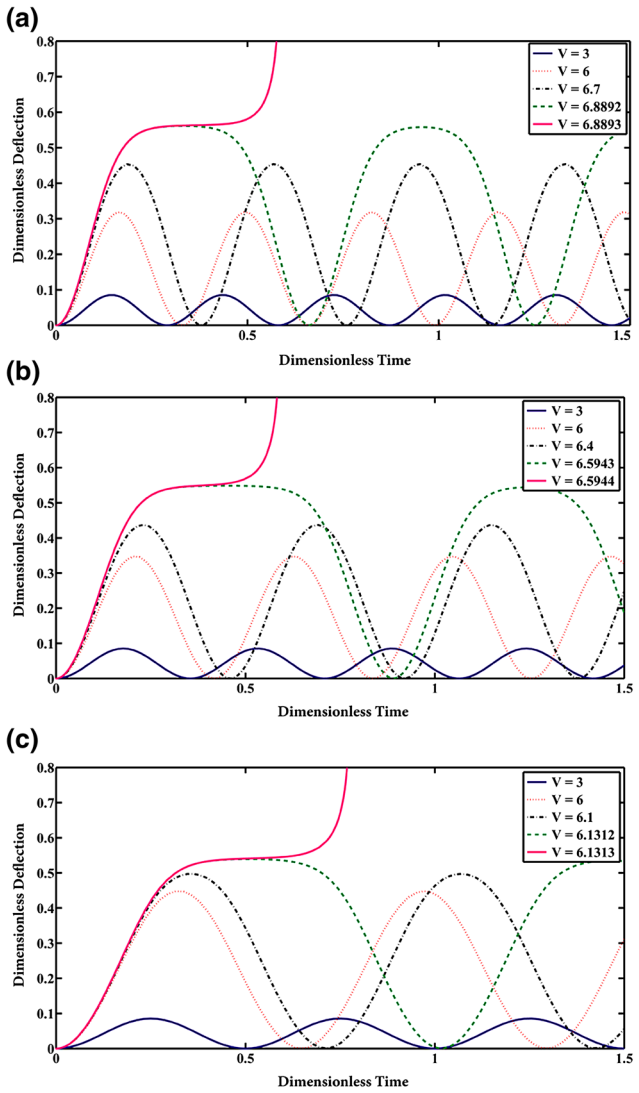

Fig. 6 **(a)** Response time history of the actuated nano-beam for various values of voltage V (a) with $(e_0a)^* = 0$. **(b)** Response time history of the actuated nano-beam for various values of voltage V (b) with $(e_0a)^* = 0.2$. **(c)** Response time history of the actuated nano-beam for various values of voltage V (c) with $(e_0a)^* = 0.4$

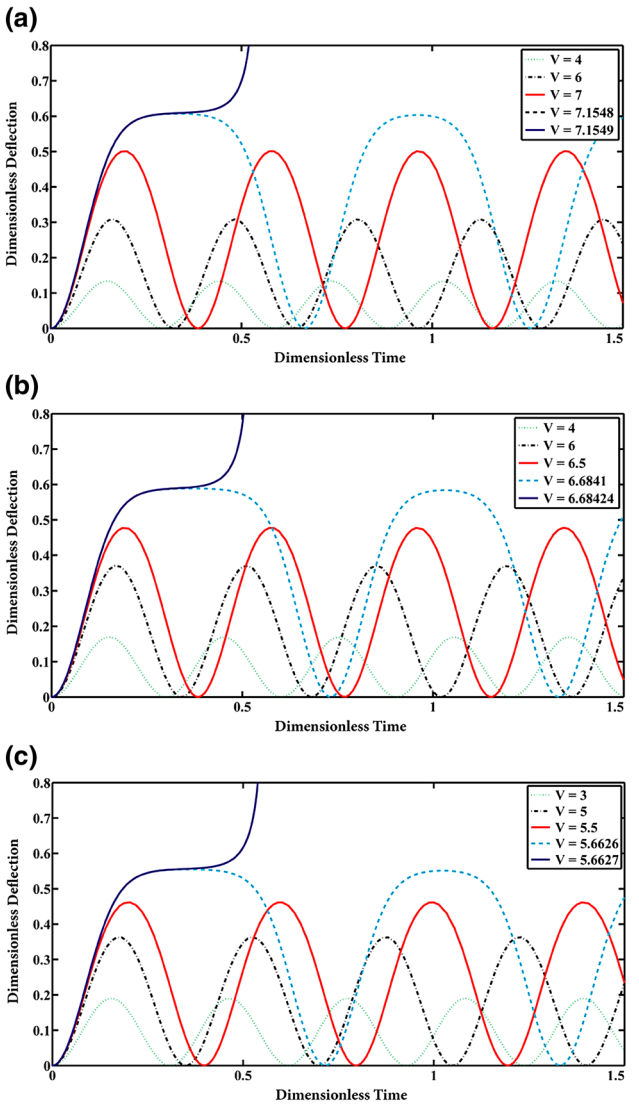

Fig. 7 **(a)** Response time history of the actuated nano-beam for various values of voltage V (a) with $\Lambda^* = 5$. **(b)** Response time history of the actuated nano-beam for various values of voltage V (b) with $\Lambda^* = 10$. **(c)** Response time history of the actuated nano-beam for various values of voltage V (c) with $\Lambda^* = 20$

4 Results and Discussion

4.1 Verification of the Present Analysis

In the considered case study, it is assumed that the nano-beam is made of silicon with $L = 510\mu m$, $h = 1.5\mu m$, $b = 100\mu m$, $d = 1.18\mu m$ and $N_i = 8.7$. Since there are no results of the pull-in voltage is calculated by the nonlocal theory in the open literature, in order to validate the results, some obtained results in the special case of $a = 0$, i.e., the results of the classical continuum theory, are compared with those presented by Rezazadeh et al [46] and Osterberg [47]. The static and dynamic pull-in voltages obtained by classical theory are tabulated in Table 1. As can be observed there is an excellent agreement between the results.

In order to validate the present analysis to estimate the dynamic behavior of the nano-resonator, the values of dynamic pull-in voltage computed by different models, are shown in Table 2 using an example of 300 μm long, 20 μm wide and 2 μm thick double clamped beam with the initial gap $d = 2\,\mu$m. The beam is assumed to be made of silicon with Young modulus $E = 169$ GPa and Poisson's ratio $\nu = 0.28$ [48]. Since the width of the beam is much larger than its thickness, the Young modulus E is replaced by $\tilde{E} = E/(1-\nu^2)$. It is obvious that the values of computed dynamic pull-in voltage (V_{pid}) agrees well with those

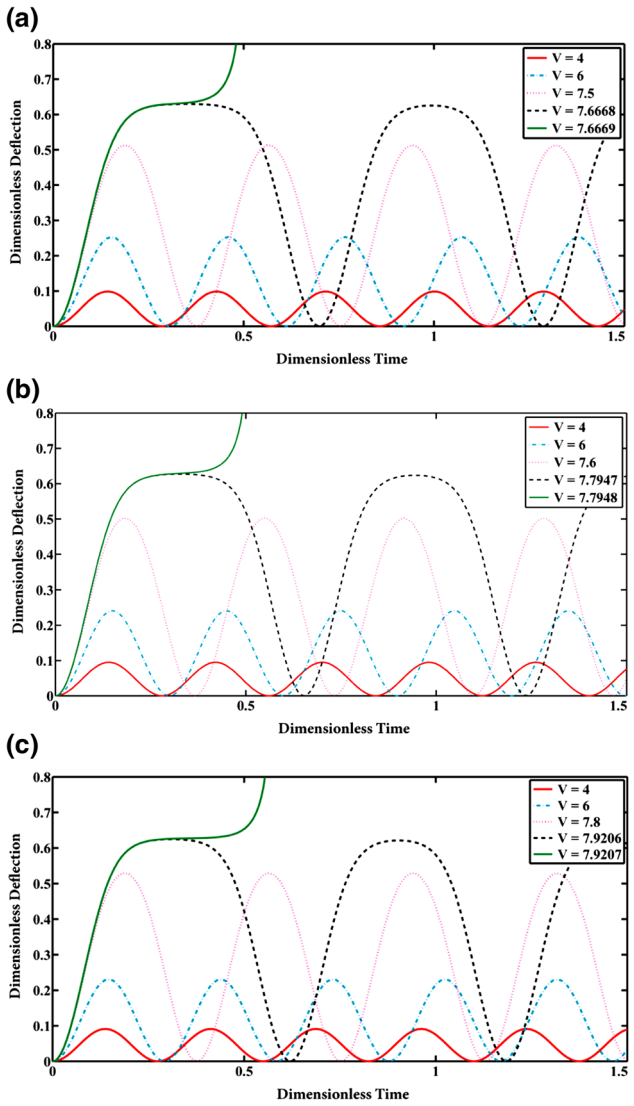

Fig. 8 **(a)** Response time history of the actuated nano-beam for various values of voltage V (a) with $k^* = 10$. **(b)** Response time history of the actuated nano-beam for various values of voltage V (b) with $k^* = 30$. **(c)** Response time history of the actuated nano-beam for various values of voltage V (c) with $k^* = 50$

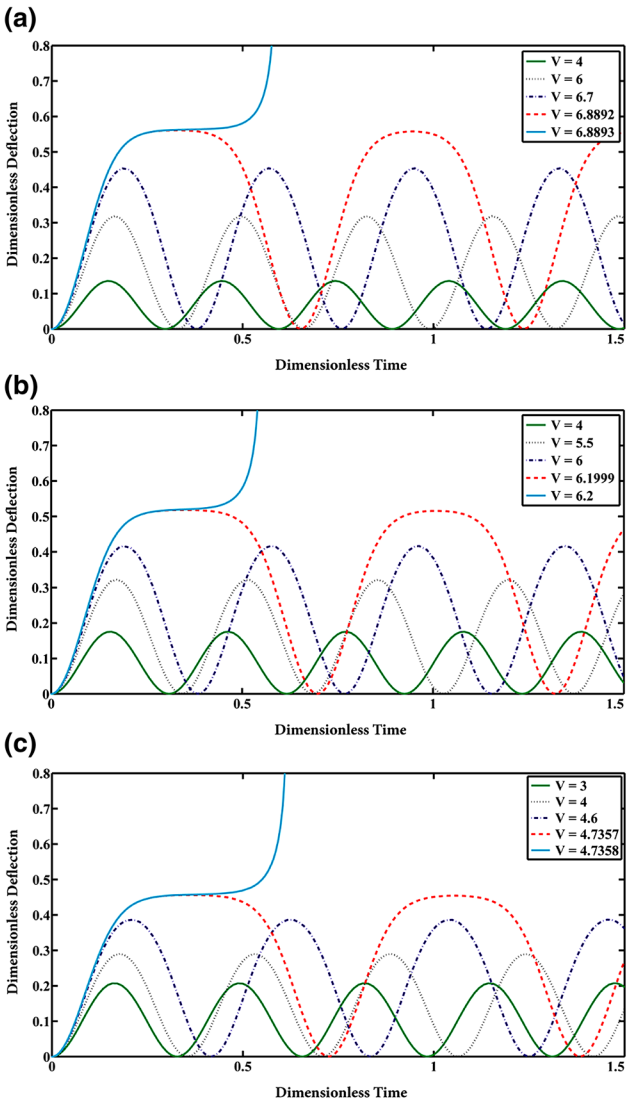

Fig. 9 **(a)** Response time history of the actuated nano-beam for various values of voltage V (a) with $(hc)^* = 5$. **(b)** Response time history of the actuated nano-beam for various values of voltage V (b) with $(hc)^* = 10$. **(c)** Response time history of the actuated nano-beam for various values of voltage V (b) with $(hc)^* = 20$

reported in the literature. Another comparison with experimental and theoretical results in the literature is performed using 100 μm wide and 1.5 μm thick micro-beams with initial gap of 1.18 μm. The effective Young's modulus for the micro-beams material is $\tilde{E} = 166$ GPa with a residual axial load $N_i = 0.0009\,N$ representative of pre-tensioned micro-beams [49]. Table 3 presents the calculated and empirical fundamental frequencies for vibrating pre-tensioned micro-bridges. This table reveals that the results of present model using PEM are in excellent agreement with the numerical and experimental results presented in the literature.

As another comparison, the dynamic pull-in voltage of a double-clamped silicon beam is considered. The geometrical properties of the beam is $L = 1000$ µm, $b = 30$ µm, $h = 2.4$ µm and $g_0 = 10.1$ µm. The material properties of the beam is $\rho = 2231$ kg/m^3, E = 97.5 GPa and $\upsilon = 0.26$ GPa. The obtained results together with those reported in literature [53, 54] are tabulated in Table 4. Krylov et al [53] measured the pull-in voltage of the micro-beam (experimentally) as 100 V. On the other hand, Das and Batra [54] also determined the pull-in voltage of this beam based on the finite element analysis. They reported that the pull-in voltage of the microbeam is between 99 V and 100 V. As can be observed in Table 4, good agreement between the present method and those of literature is achieved.

4.2 Numerical results

In this section, the numerical results for static and dynamic behavior of nano-bridge actuators are presented. Fig. 2 shows the effect of normalized internal parameter $(e_0a)^*$ on the curves of maximum static deflection versus the normalized input voltage V_0^* for $b/d = 5$ and $k^* = 1$. From Fig. 2, it is noted that the case with $(e_0a)^* = 0$ yields the results of the classical beam theory. Moreover, the static pull-in voltages predicted by the nonlocal theory are smaller than those of the classical continuum theory.

Figure 3 demonstrates the effect of aspect ratio d/b on the variation of maximum dimensionless deflection versus normalized input voltage V_0^* for $(e_0a)^* = 0.2$ and $k^* = 1$. From Fig. 3, it can be founded that the values of static pull-in voltage are strongly dependent to aspect ratio d/b, as well as with increase in this aspect ratio, the values of static pull-in voltage are reduced notably. Fig. 4 represents the effect of Casimir parameter $(\mathrm{hc})^*$ on the variation of maximum dimensionless deflection versus normalized input voltage V_0^* for $(e_0a)^* = 0.2$ and $k^* = 1$. As can be seen, the values of static pull-in voltage remarkably reduce with rise of the Casimir parameter.

Figure 5 illustrates the effect of van der Waals parameter Λ^* on the variation of maximum dimensionless deflection versus normalized input voltage V_0^* for $(e_0a)^* = 0.2$ and $k^* = 1$. It can be concluded that when the van der Waals parameter Λ^* increases, the static pull-in voltage decreases significantly. Comparing with Figs. 4 and 5, the effect of Casimir intermolecular force on the static pull-in behavior is the more remarkable than kind of van der Waals.

Here, the numerical results are given the dynamic pull-in analysis of the actuated nano-beam with with $k^* = 1, \alpha = 6, N_i = 1$. Fig. 6 displays the effect of normalized internal parameter $(e_0a)^*$ on the response time history of the actuated nano-beam for various values of applied voltage. It is noticed from Figs. 6*a*, 6*b* and 6*c* that the values of dynamic pull-in voltage decreases continuously as the value of normalized internal parameter becomes larger.

Figure 7 exhibits the effect of van der Waals parameter Λ^* on the response time history for a range of voltages. From Figs. 7*a*, 7*b* and 7*c*, it can be concluded that when van der Waals parameter Λ^* increases, the values of dynamic pull-in voltage reduce so slightly.

Figure 8 compares the responses time history obtained by numerical simulations for various values of the stiffness parameter k^* and voltage V. It can be observed from Figs. 8*a*, 8*b* and 8*c* that the dynamic pull-in voltages get larger with increase in values of stiffness parameter. Fig. 9 presents the dynamic behavior of nano-resonators for different values of Casimir parameter $(\mathrm{hc})^*$ and actuation voltage V. From Figs. 9*a*, 9*b* and 9*c*, it can be found that the dynamic pull-in voltages decrease by increasing the Casimir parameter $(\mathrm{hc})^*$. By comparison between Figs. 7 with 9, it can be readily concluded that the effects of van der Waals and Casimir intermolecular forces are to reduce the dynamic pull-in voltage of the nano-structure.

5 Conclusion

In this study, the static and dynamic pull-in behaviors of nano-beams resting on the elastic foundation were investigated by employing the nonlocal elasticity theory. The governing equation of motion included the influences of fringing field and intermolecular forces such as Casimir and van der Waals forces. The differential quadrature method and Parameter Expansion Method were utilized to solve the static and dynamic governing equations. Finally, the effects of basic parameters including the normalized internal parameter, van der Waals parameter, the Casimir and stiffness parameter on the static and dynamic pull-in behavior were studied.

Appendix A

$$\beta_i = \frac{\beta_i'}{\left(1 - (e_0a)^{*2}\int_0^1 \phi\phi''d\xi\right)}, \quad i = 0,1,2,3,4$$

For van der Waals intermolecular force:

$$\beta_0' = -\left((V_0^*)^2(1+\hat{f}^*) + \Lambda^*\right)\int_0^1 \phi d\xi$$

$$\beta_1' = \lambda^4 - \left((V_0^*)^2(2+\hat{f}^*) + 3\Lambda^*\right)$$
$$\int_0^1 \left(\phi^2 - (e_0a)^{*2}\phi\phi''\right)d\xi - f_i\int_0^1 \left(\phi\phi'' - (e_0a)^{*2}\phi\phi^{(4)}\right)d\xi$$

$$\beta_2' = -\left((V_0^*)^2(3+\hat{f}^*) + 6\Lambda^*\right)\int_0^1 \left(\phi^3 - (e_0a)^{*2}\phi(\phi^2)''\right)d\xi$$

$$\beta_3' = -\left((V_0^*)^2(4+\hat{f}^*) + 10\Lambda^*\right)\int_0^1 \left(\phi^4 - (e_0a)^{*2}\phi(\phi^3)''\right)d\xi$$
$$-\alpha\left[\left(\int_0^1 \left(\phi\phi''\left[\int_0^1 \phi'^2 d\xi\right] - (e_0a)^{*2}\phi\left(\phi''\left[\int_0^1 \phi'^2 d\xi\right]\right)''\right)d\xi\right)\right]$$

$$\beta_4' = -\left((V_0^*)^2(5+\hat{f}^*) + 15\Lambda^*\right)\int_0^1 \left(\phi^5 - (e_0a)^{*2}\phi(\phi^4)''\right)d\xi$$

(A – 1)

For Casimir intermolecular force:

$$\beta_0' = -\left((V_0^*)^2(1+\hat{f}^*) + (\hbar c)^*\right)\int_0^1 \phi d\xi$$

$$\beta_1' = \lambda^4 - \left((V_0^*)^2(2+\hat{f}^*) + 4(\hbar c)^*\right)$$

$$\int_0^1 \left(\phi^2 - (e_0a)^{*2}\phi\phi''\right)d\xi - f_i\int_0^1 \left(\phi\phi'' - (e_0a)^{*2}\phi\phi^{(4)}\right)d\xi$$

$$\beta_2' = -\left((V_0^*)^2(3+\hat{f}^*) + 10(\hbar c)^*\right)\int_0^1 \left(\phi^3 - (e_0a)^{*2}\phi(\phi^2)''\right)d\xi$$

$$\beta_3' = -\left((V_0^*)^2(4+\hat{f}^*) + 20(\hbar c)^*\right)\int_0^1 \left(\phi^4 - (e_0a)^{*2}\phi(\phi^3)''\right)d\xi$$

$$-\alpha\left[\left(\int_0^1\left(\phi\phi''\left[\int_0^1 \phi'^2 d\xi\right] - (e_0a)^{*2}\phi\left(\phi''\left[\int_0^1 \phi'^2 d\xi\right]\right)''\right)d\xi\right)\right]$$

$$\beta_4' = -\left((V_0^*)^2(5+\hat{f}^*) + 35(\hbar c)^*\right)\int_0^1 \left(\phi^5 - (e_0a)^{*2}\phi(\phi^4)''\right)d\xi \qquad (A-2)$$

References

1. Faris WF, Abdel-Rahman EM, Nayfeh AH. Mechanical behavior of an electro statically actuated micro pump. Proc. 43rd AIAA/ASME/ASCE/AHS/ASC, Structures, Structural Dynamics, and Materials Conference, AIAA, 2002, 1003.
2. Zhang XM, Chau FS, Quan C, Lam YL, Liu AQ. A study of the static characteristics of a torsional micromirror. Sensors and Actuators A: Physical Journal, 2001, 90(2): 73–81.
3. Zhao X, Abdel-Rahman EM, Nayfeh AH. A reduced-order model for electrically actuated micro plates. Micro mechanics and Micro engineering Journal, 2004, 14: 900–906.
4. Tilmans HA, Legtenberg R. Electro statically driven vacuum-encapsulated poly silicon resonators: part II. Theory and performance. Sensors and Actuators A, 1994, 45: 67–84.
5. Ghalambaz, M., Ghalambaz, M., Edalatifar, M. Nonlinear oscillation of nanoelectro-mechanical resonators using energy balance method: considering the size effect and the van der Waals force, Appl Nanosci, 2016, DOI 10.1007/s13204-015-0445-3.
6. Parsediya, D.K., Singh, J., Kankar, P.K. Variable width based stepped MEMS cantilevers for micro or pico level biosensing and effective switching, Journal of Mechanical Science and Technology, 2015, 29(11): 4823–4832.
7. Shoaib, M., Hisham, N., Basheer, N., Tariq, M. Frequency and displacement analysis of electrostatic cantilever based MEMS sensor, Analog Integr Circ Sig Process, 2016, DOI 10.1007/s10470-016-0695-3.
8. Canadija, M, Barretta, R, Marotti de Sciarra, F. On Functionally Graded Timoshenko Nonisothermal Nanobeams. Composite Structures, 2016, 135: 286–296.
9. Barretta R, Feo, L, Luciano, R. Torsion of functionally graded nonlocal viscoelastic circular nanobeams. Composites: Part B, 2015, 72: 217–222.
10. Barretta, R, Feo, L, Luciano, R, Marotti de Sciarra, F. Variational formulations for functionally graded nonlocal Bernoulli-Euler nanobeams. Composite Structures, 2015, 129: 80–89.
11. Sedighi, H.M., Keivani, M., Abadyan, M. Modified continuum model for stability analysis of asymmetric FGM double-sided NEMS: Corrections due to finite conductivity, surface energy and nonlocal effect. Composites Part B Engineering, 2015, 83: 117–133. DOI:10.1016/j.compositesb.2015.08.029.
12. Barretta, R, Feo, L, Luciano, R, Marotti de Sciarra, F. A gradient Eringen model for functionally graded nanorods. Composite Structures, 2015, 131: 1124–1131.
13. Čanađija, M., Barretta, R., Marotti de Sciarra, F. A gradient elasticity model of Bernoulli-Euler nanobeams in nonisothermal environments. European Journal of Mechanics A/Solids, 2015, 55: 243–255.
14. Zand MM, Ahmadian MT. Dynamic pull-in instability of electrostatically actuated beams incorporating Casimir and van der Waals forces. Proc. IMechE Part C: J. Mechanical Engineering Science, 224: 2037–47.
15. Sadeghian, H., Rezazadeh, G., Osterberg, P.M. Application of the Generalized Differential Quadrature Method to the Study of Pull-In Phenomena of MEMS Switches. Journal of microelectromechanical system, 2015, 16(6): 1334–1340.
16. Hsu, M.H. Electromechanical analysis of electrostatic nano-actuators using the differential quadrature method. Commun. Numer. Meth. Engng, 2008, 24: 1445–1457.
17. Sedighi, H.M., Shirazi, K.H. Vibrations of micro-beams actuated by an electric field via parameter expansion method. Acta Astronautica, 2013, 85: 19–24.
18. Zare, J. Pull-in behavior analysis of vibrating functionally graded micro-cantilevers under suddenly DC voltage. Journal of Applied and Computational Mechanics, 2015, 1(1): 17–25.
19. Sedighi, H. M. Daneshmand, F. Yaghootian, A. Application of Iteration Perturbation Method in studying dynamic pull-in instability of micro-beams. Latin American Journal of Solids and Structures, 2014, 11: 1078–1089.
20. Ale Ali, N., Karami Mohammadi, A. Effect of thermoelastic damping in nonlinear beam model of MEMS resonators by differential quadrature method. Journal of Applied and Computational Mechanics, 2015, 1(3): 112–121.
21. Edalatzadeh, M.S., Alasty, A. Boundary exponential stabilization of non-classical micro/nano beams subjected to nonlinear distributed forces. Applied Mathematical Modelling, 2016, 40(3): 2223–2241.
22. Fleck NA, Muller GM, Ashby MF, Hutchinson JW. Strain gradient plasticity: theory and experiment. Acta Metallurgica et Material Journal, 1994, 42(2): 475–487.
23. Stolken JS, Evans AG. Micro bend test method for measuring the plasticity length scale. Acta Materialia Journal, 1998, 46(14): 5109–5115.
24. Eringen, A.C. Nonlocal polar elastic continua, Int. J. Eng. Sci., 1982, 10: 1–16.
25. Lam, D. C. C., Yang, F., Chong, A. C. M., Wang, J., Tong, P. Experiments and theory in strain gradient elasticity.Journal of the Mechanics and Physics of Solids, 2003, 51, 1477–1508.
26. Toupin RA. Elastic materials with couple-stresses. Arch. Ration. Mech. Anal, 1962, 11(1):385–414.
27. Patti, A., Barretta, R., Marotti de Sciarra, F., Mensitieri G., Menna C., Russo P. Flexural properties of multi-wall carbon nanotube/polypropylene composites: Experimental investigation and nonlocal modeling. Composite Structures, 2015, 131: 282–289.
28. Barretta R., Marotti de Sciarra F. Analogies between nonlocal and local Bernoulli-Euler nanobeams. Archive of Applied Mechanics, 2015, 85(1): 89–99.
29. Edalatzadeh, M.S., Vatankhah, R., Alasty, A. Suppression of Dynamic Pull-in Instability in Electrostatically Actuated Strain Gradient Beams, Proceeding of the 2nd ISI/ISM International

Conference on Robotics and Mechatronics, October 15–17, 2014, Tehran, Iran.
30. Shojaeian, M., Tadi Beni, Y., Ataei, H. Electromechanical Buckling of Functionally Graded Electrostatic Nanobridges Using Strain Gradient Theory, Acta Astronautica, 2016, doi: 10.1016/j.actaastro.2015.09.015.
31. Tadi Beni, Y., Mehralian, F., Zeighampour, H. The modified couple stress functionally graded cylindrical thin shell formulation, Mechanics of Advanced Materials and Structures, 2016, 23: 791–801.
32. Mojahedi, M., Rahaeifard, M., Static Deflection and Pull-In Instability of the Electrostatically Actuated Bilayer Microcantilever Beams, International Journal of Applied Mechanics, 2015, 7(6): 1550090.
33. Molaei M, Ahmadian MT, Taati E. Effect of thermal wave propagation on thermoelastic behavior of functionally graded materials in a slab symmetrically surface heated using analytical modeling. Composites: Part B, 2014, 60:413–422.
34. MolaeiM, TaatiE, Basirat H. Optimization of functionally graded materials in the slab symmetrically surface heated using transient analytical solution. Journal of Thermal Stresses, 2014, 37: 137–159.
35. Sedighi, H. M., Koochi, A., Abadyan, M.R. Modeling the size dependent static and dynamic pull-in stability of cantilever nano-actuator based on the strain gradient theory, International Journal of Applied Mechanics, 2014, 6(5).
36. Sedighi, H. M. Daneshmand, F. Abadyan, M.R. Modified model for instability analysis of symmetric FGM double-sided nano-bridge: Corrections due to surface layer, finite conductivity and size effect. Composite Structures, 2015, 132, 545–557.
37. Sedighi, H. M., Koochi, A., Daneshmand, F., Abadyan, M.R. Non-linear dynamic instability of a double-sided nano-bridge considering centrifugal force and rarefied gas flow. International Journal of Non-Linear Mechanics, 2015, 77: 96–106.
38. Sedighi, H. M., Changizian, M., Noghrehabadi, A. Dynamic pull-in instability of geometrically nonlinear actuated micro-beams based on the modified couple stress theory. Latin American Journal of Solids and Structures, 2014, 11: 810–825.
39. Tadi Beni, Y. Size-dependent electromechanical bending, buckling, and free vibration analysis of functionally graded piezoelectric nanobeams. Journal of Intelligent Material Systems and Structures, 2016, doi: 10.1177/1045389X15624798.
40. Barretta, R., Feo, L., Luciano, R., Marotti de Sciarra, F. An Eringen-like model for Timoshenko nanobeams. Composite Structures, 2016, 139: 104–110.
41. Karimi, M., Shokrani, M.H., Shahidi, A.R. Size-dependent free vibration analysis of rectangular nanoplates with the consideration of surface effects using finite difference method. Journal of Applied and Computational Mechanics, 2015, 1(3): 122–133.
42. Sedighi, H.M., Bozorgmehri, A. Nonlinear vibration and adhesion instability of Casimir-induced nonlocal nanowires with the consideration of surface energy, Journal of the Brazilian Society of Mechanical Sciences and Engineering, 2016, doi: 10.1007/s40430-016-0530-x.
43. Karimipour, I., Tadi Beni, Y., Koochi, A., Abadyan, M. Using couple stress theory for modeling the size-dependent instability of double-sided beam-type nanoactuators in the presence of Casimir force. Journal of the Brazilian Society of Mechanical Sciences and Engineering, 2016, doi: 10.1007/s40430-015-0385-6.
44. Sheikhanzadeh, A., Sedighi, H.M. Static and Dynamic pull-in instability of nano-beams resting on elastic foundation using the Differential Quadrature Element Method, Master Thesis, Najafabad Branch, Islamic Azad Univesity, Najafabad, Iran, 2015.
45. Reddy, J.N. Nonlocal nonlinear formulations for bending of classical and shear deformation theories of beams and plates. Int J Eng Sci, 2010, 48: 1507–18.
46. Rezazadeh, G., Fathalilou, M., Morteza Sadeghi. Pull-in Voltage of Electrostatically-Actuated Microbeams in Terms of Lumped Model Pull-in Voltage Using Novel Design Corrective Coefficients, Sens Imaging, 2011, 12: 117–131.
47. Osterberg, P. Electrostatically actuated microelectromechanical test structures for material property measurement, Ph.D. thesis, MIT, Cambridge, 1995.
48. Krylov, S. Lyapunov exponents as a criterion for the dynamic pull-in instability of electrostatically actuated microstructures, Int. J. Non-Linear Mech., 2007, 42: 626–642.
49. Tilmans, H.A., Legtenberg, R., Electrostatically driven vacuum-encapsulated polysilicon resonators. Part II: theory and performance, Sens. Actuat. A, 1994, 45(1): 67–84.
50. Sedighi, H.M., Daneshmand, F., Abadyan, M. Modeling the effects of material properties on the pull-in instability of nonlocal functionally graded nano-actuators, Z. Angew. Math. Mech. 2016, 96(3): 385–400.
51. Kuang, J.H., Chen, C.J. Dynamic characteristics of shaped micro-actuators solved using the differential quadrature method. J. Micromech. Microeng., 2004, 14(4): 647–655.
52. Moghimi Zand, M., Ahmadian, M.T. Application of homotopy analysis method in studying dynamic pull-in instability of Microsystems, Mechanics Research Communications, 2009, 36: 851–858
53. Krylov, S., Ilic, B.R., Schreiber, D., Seretensky, S., Craighead, H. The pull-in behavior of electrostatically actuated bistable microstructures, Journal of Micromechanics and Microengineering, 2008, 18, 055026 (20 pp)
54. Das, K., Batra, R.C. Pull-in and snap-through instabilities in transient deformations of microelectromechanical systems, Journal of Micromechanics and Microengineering, 2009, 19, 035008 (19 pp).

HAMID M Sedighi was born in 1983 in Iran. He is currently a member of engineering faculty at Shahid Chamran University of Ahvaz in Iran. He obtained his PhD degree (2013) from Shahid Chamran University, M.S. degree (2007) from the Shahid Chamran University and his undergraduate B.S. degree (2005) from the Shiraz University. His general academic areas of interest include the applied mathematics, nonlinear dynamical systems, MEMS/NEMS and machine design. Tel: +98 61133 30010x5665-; Fax: +98 611333 6642.

ASHKAN Sheikhanzadeh was born in Iran. He obtained his M.S. degree from Islamic Azad Univesity, Najafabad Branch, Iran. His general academic areas of interest include the numerical methods, applied mathematics and MEMS/NEMS.